Composites: Part A 158 (2022) 106931

Contents lists available at ScienceDirect

Composites Part A

journal homepage: www.elsevier.com/locate/compositesa

Rapid multiple-front polymerization of fiber-reinforced polymer composites

P.J. Centellas [a,b], M. Yourdkhani [a,d], S. Vyas [a,b], B. Koohbor [a,e], P.H. Geubelle [a,b], N.R. Sottos [a,c,*]

[a] Beckman Institute for Advanced Science and Technology, University of Illinois, Urbana, IL, 61801, United States
[b] Department of Aerospace Engineering, University of Illinois, Urbana, IL, 61801, United States
[c] Department of Materials Science and Engineering, University of Illinois, Urbana, IL, 61801, United States
[d] Department of Mechanical Engineering, Colorado State University, Fort Collins, CO, 80523, United States
[e] Department of Mechanical Engineering, Rowan University, Glassboro, NJ, 08028, United States

ARTICLE INFO

Keywords:
A. Polymer–matrix composites (PMCs)
D. Mechanical testing
E. Out of autoclave processing
Frontal polymerization

ABSTRACT

Frontal polymerization (FP) is an out-of-autoclave, self-sustaining cure process that enables rapid and energy-efficient manufacturing of composites compared to conventional processes. Prior FP demonstrations for both polymer and composite materials rely on one polymerization front to achieve full cure. In this work, we investigate the effect of multiple polymerization fronts on the composite cure time, quality, and mechanical performance. Localized void formation, panel thickness increase, and thermal spike are measured between two merging fronts and observed to have a detrimental impact on composite performance. Numerical simulations guide the mitigation of the thermal spike by modifying the layup from thermally insulated boundaries (TIB) to thermally conductive boundaries (TCB). Panels manufactured with TCB successfully mitigate all adverse phenomena at the merging fronts, leading to improved composite mechanical properties. A 5-fold reduction in cure time from ca. 5 min for one-front TIB panels to ca. 1 min for two-front TCB panels is achieved.

1. Introduction

The use of thermoset composites as structural components continues to grow across transportation and energy sectors due to robust mechanical, thermal, and chemical properties for reduced weight [1–4]. Despite these benefits, the equipment, energy, and time demands associated with composite manufacturing [5–7] drive up cost and limit market growth [8–10].

Strategies that exploit 'snap-cure' resins [11–14], heated molds [15–17], and frontal polymerization (FP) [18–24] shorten the composite cure cycle from hours to minutes compared to conventional bulk curing. Snap-cure resins and heated molds require a constant external energy source to achieve sufficiently high temperatures to fully cure the composite matrix. The size of the composite part is thereby limited by the size of the external energy source. In contrast, frontal polymerization (FP) is a fast and self-driven curing process sustained by the exothermic polymerization of the matrix. The FP process is initiated by a local heat trigger that polymerizes the matrix monomer. Heat produced from the initial reaction polymerizes adjacent monomer, forming a self-propagating polymerization wave or front. Previously, we demonstrated the rapid FP of carbon–fiber-reinforced polymer (CFRP) composites using one and two in-plane heat triggers as well as a through-thickness heat trigger [21]. Use of multiple triggers (i.e. fronts) achieved faster composite cure times compared to the one-trigger case [21], encouraging further investigation into multiple-front polymerization [25].

Faster cure times achieved by multiple fronts have potential application for manufacturing larger composites and higher volumes of production. Since the FP process does not require external energy input beyond the initial heat trigger, multiple-front polymerization also promises significant energy savings. No reports thus far have studied the effect of multiple fronts on the cured components.

Here, we investigate the quality and performance of CFRP composites cured by multiple-front polymerization. Composite front characteristics (temperature and velocity), cure time, quality (void content and thickness uniformity), and performance (glass transition temperature and tensile properties) are evaluated for one-front and two-front trigger configurations and compared to a conventional bulk-cured aerospace-grade epoxy composite. The merging location of multiple fronts is also modeled computationally and predictions helped understand the role of thermally insulated or thermally conductive boundaries for producing high quality composites.

* Corresponding author at: Department of Materials Science and Engineering, University of Illinois, Urbana, IL, 61801, United States.
E-mail address: n-sottos@illinois.edu (N.R. Sottos).

https://doi.org/10.1016/j.compositesa.2022.106931
Received 9 November 2021; Received in revised form 9 March 2022; Accepted 16 March 2022
Available online 31 March 2022
1359-835X/

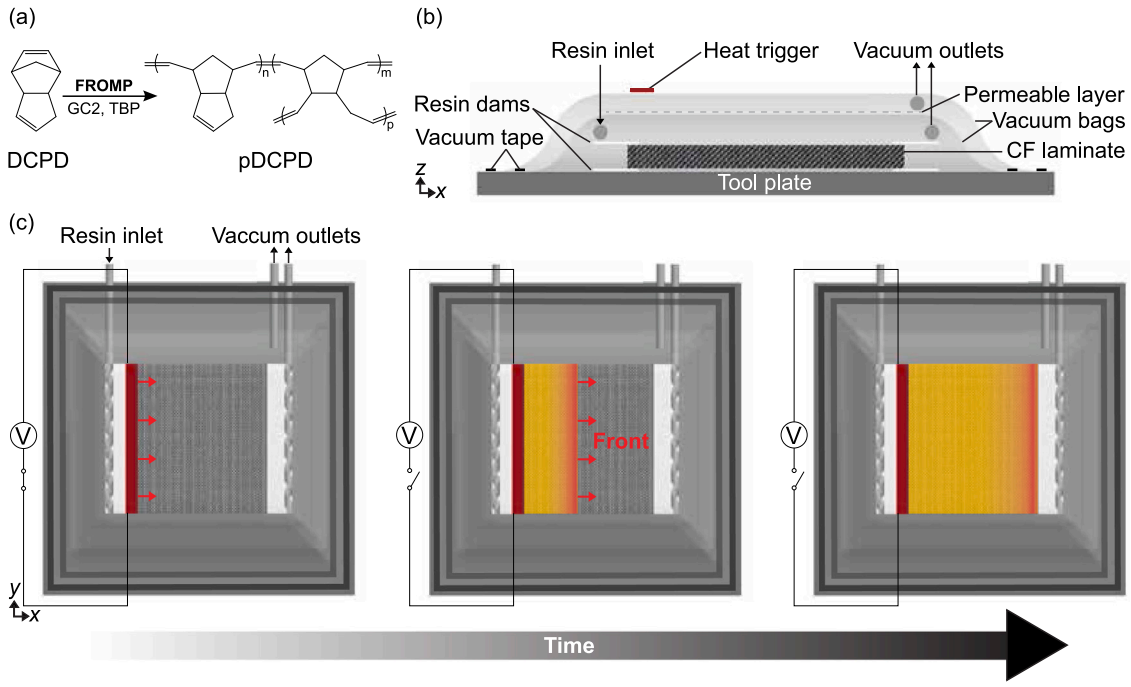

Fig. 1. Composite manufacturing via frontal polymerization (FP). (a) Scheme for frontal ring-opening metathesis polymerization (FROMP) of dicyclopentadiene (DCPD)-based liquid resin. (b) Side view and (c) top view schematic representation of double-bag vacuum-assisted resin transfer molding (VARTM) layup drawn to scale. Woven fabric is infused with liquid DCPD resin. A resistive heater is briefly powered to initiate a polymerization front.

2. Methodology

2.1. Materials

A low-viscosity resin based on dicyclopentadiene was used for all FP composites and prepared according to the procedure outlined by Robertson et al. [21]. Dicyclopentadiene (DCPD), 5-ethylidene-2-norbornene (ENB), second-generation Grubbs' catalyst (GC2), phenylcyclohexane (PCH), and tributyl phosphite inhibitor (TBP) were purchased from Sigma-Aldrich and used as received without further purification. DCPD was first melted in an oven at 50 °C, then mixed with 5 wt% ENB to depress its melting point. We refer to this 95/5 DCPD/ENB solution as DCPD resin hereafter. The resin was then degassed at 100 kPa vacuum pressure overnight. In a separate container, 115 mg of GC2 was dissolved in 5.75 mL of PCH in a sonication bath for 40 min. We then added 10 μL of TBP (0.3 molar equivalent with respect to GC2) to the sonicated solution. The solution was mixed with 180 g of the DCPD resin (10,000 molar equivalents with respect to GC2). Once prepared, the resin solution was immediately infused into the composite layup. A heat trigger initiated the frontal ring-opening metathesis polymerization (FROMP) of DCPD into fully crosslinked polydicyclopentadiene (pDCPD) (Fig. 1a).

2.2. Double-bag vacuum-assisted resin-transfer molding (VARTM) layup

All composites were fabricated using a double-bag vacuum-assisted resin-transfer molding (VARTM) processing technique with 12 plies of 30×30 cm^2 Toray T300 carbon fiber fabric (2×2 twill weave, tow size 3,000, areal density 204 g m^{-2}). The VARTM layup was prepared on a flat tool plate of variable material. A vacuum equal to 6.5 kPa (absolute pressure) was applied on the inner bag using a vacuum pump to infuse the dry carbon fiber (CF) laminate with the liquid resin solution. A stronger vacuum of 0.05 kPa (absolute pressure) was applied on the outer bag using a second vacuum pump to compact the laminate and produce composites with ca. 50% fiber volume fraction. One or more flexible resistive heaters (2.5 × 30 cm^2, OMEGALUX®, model SRFG-112/10, 120 W) were connected to an AC power supply (Staco Energy Products Co., model L1010) and secured on the surface of the VARTM layup (Fig. 1b). Once the resin infused the fabric, the heater(s) were powered for ca. 35 s to initiate polymerization. After FROMP was initiated, the power was turned off and polymerization front(s) self-propagated through the remaining laminate volume (Fig. 1c).

2.3. FROMP with thermally insulated boundaries (TIB)

One-front and two-front composite panels were fabricated using the double-bag VARTM layup with thermally insulated boundaries (TIB). The VARTM layup was prepared on an insulator tool plate (448-D, Fibre Glast Developments Corp., thermal conductivity = 0.03 W m^{-1} K^{-1}, thermal diffusivity = 0.2 mm^2 s^{-1}, 25 mm thick) and the experiments were carried out at room temperature (Fig. 2a, b). The low thermal conductivity (κ) and diffusivity (λ) of the insulator plate and ambient air minimized heat losses during cure and prevented quenching of the front.

The two-front test was accomplished by connecting two identical resistive heaters in parallel to a power supply and securing them onto the layup surface at opposing ends, i.e. near the resin inlet and vacuum outlet (Fig. 2b). Once the dry laminate was infused with the liquid resin solution, both heaters were briefly powered to initiate two linear polymerization fronts. The two traveling fronts converged at the mid-length of the 30 cm long laminate; hereafter, this region is referred to as the merged interface.

2.4. FROMP with thermally conductive boundaries (TCB)

Two-front composites were also prepared using the double-bag VARTM layup with thermally conductive boundaries (TCB). The VARTM layup was prepared on an aluminum plate (κ = 202 W m^{-1} K^{-1}, λ = 85 mm^2 s^{-1}, 6 mm thick) and then preheated to ca. 45 °C. The preheated layup was then infused with the room temperature resin solution. After infusion, a second preheated aluminum plate (at ca. 45 °C) was placed on top of the layup to apply an external pressure (P) of 0.6 kPa onto the layup surface (Fig. 3). Once the two fronts were initiated, the resin temperature (T_o) was tracked during the cure

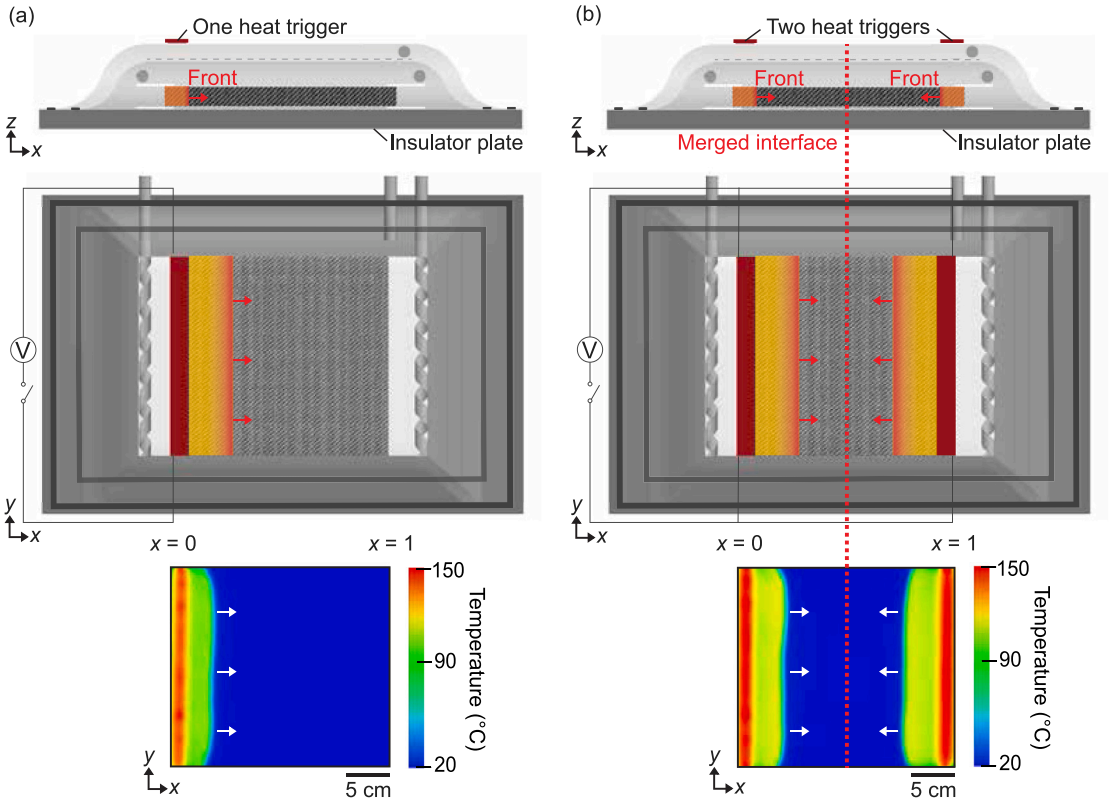

Fig. 2. Side view (first row) and top view (second row) schematic representations of (a) one- and (b) two-heat-trigger layups with thermally insulated boundaries (TIB). Powering two heat triggers initiates two simultaneous fronts near the resin inlet (normalized length, $x = 0$) and outlet ($x = 1$) that merge at the panel mid-length ($x = 0.5$), i.e. the merged interface (dotted red line). The propagation of the exothermic fronts (in the direction of the white arrows) was visualized using an infrared camera focused on the layup surface (third row).

process by thermocouples secured on the CF laminate surface. The targeted T_o was determined experimentally; when $T_o \leq 30$ °C the two fronts quenched and when $T_o \geq 50$ °C the laminate underwent bulk polymerization. Therefore, the target T_o was selected as 40 °C (measured $T_o = 42 \pm 1.2$ °C) for all TCB tests.

2.5. Bulk cure of epoxy composites

The FROMP composite panels were compared to the bulk-cured pDCPD and aerospace-grade bisphenol A epoxy composites reported in our previous work [21]. Bulk-cured pDCPD composites were comprised of the same constituents used in FROMP experiments and fabricated via a conventional wet layup technique. The panels were cured in a hydraulic press (MTP-13, Tetrahedron) for 24 h at room temperature, 2 h at 70 °C, and 1.5 h at 170 °C. The resin matrix used for epoxy composites was a solution of Araldite LY 8605 resin and Aradur 8605 hardener (100/35 weight ratio) and the reinforcement was the same CF used in FROMP experiments. Panels were fabricated using a conventional wet layup technique and cured in a hydraulic press (MTP-13, Tetrahedron). The cure cycle was 24 h at room temperature, 2 h at 121 °C, and 3 h at 177 °C.

2.6. Material characterization

Temperature was measured *in-situ* during FROMP curing with T-type thermocouples (TMQSS, Omega) embedded on the top surface of the CF laminate and spaced 1.5 cm apart. The peak temperature recorded by each thermocouple was defined as the front temperature (T_{front}) at that thermocouple position. The velocity of the front propagation was calculated from the slope of the best-fit trendline (m) for front position versus time data (Fig. 4). The cure time was defined as the time required for the front to progress from the resin inlet to the vacuum outlet for one-front cases or to the panel mid-length for two-front cases.

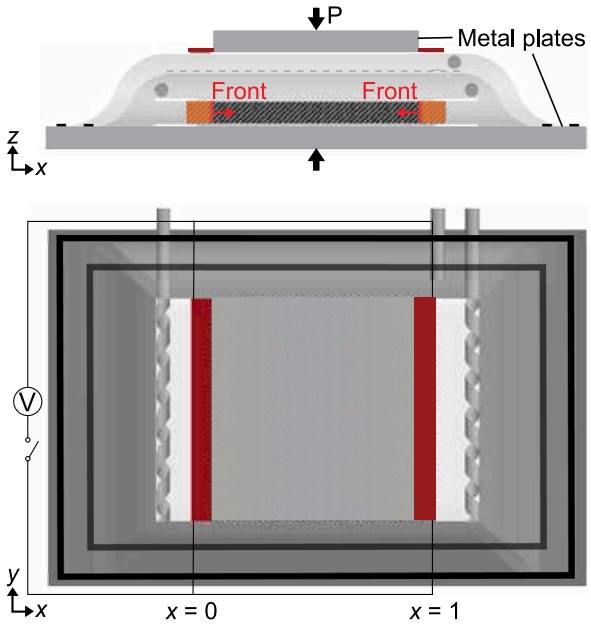

Fig. 3. Side view (top row) and top view (bottom row) schematic representations of two-front composites prepared using a VARTM layup with thermally conductive boundaries (TCB) by replacing the insulator tooling with two aluminum plates.

Table 1
Comparison of tensile strength for FROMP specimens.[a]

Specimen	Number of specimen	Fiber volume fraction (%)	Tensile strength (MPa)
One front TIB	17	52.0 ± 0.2	618 ± 12
Two fronts TIB	17	47.3 ± 0.5[b]	557 ± 22
Two fronts TCB	12	49.5 ± 0.1	656 ± 12
Bulk-cured pDCPD [21]	10	51.1 ± 1.3	672 ± 12
Bulk-cured epoxy [21]	8	52.2 ± 1.2	748 ± 50

[a]Error represents one standard deviation.
[b]Fiber volume fraction near the panel outlet. Lower fiber volume fraction of 42.8 ± 0.4% calculated near the merged interface due to the formation of a resin rich layer on the composite surface.

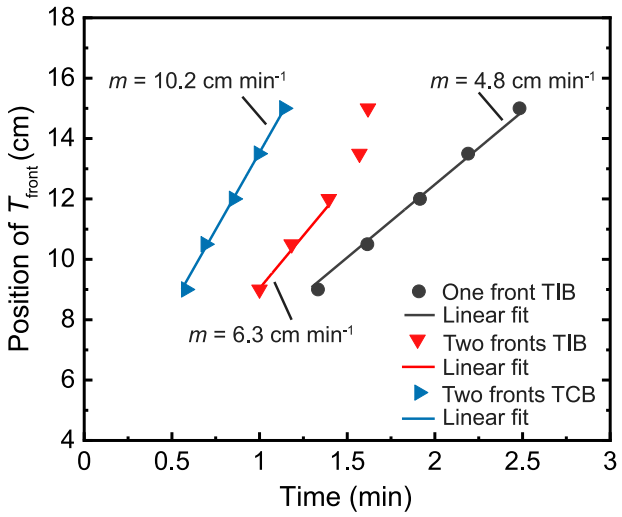

Fig. 4. Position of the front as a function of time for one-front TIB (gray), two-front TIB (red), and two-front TCB (blue) representative composites. The slope of the linear fit (m) was defined as the front velocity. The two-front TIB panel showed an increase in front velocity as the front neared the merged interface (located at 15 cm).

Void content of the cured composites was measured on polished cross-sections of 30 mm × 10 mm samples cut along the panel length and imaged with an optical digital microscope (VHX-5000, Keyence). ImageJ software was used to calculate the ratio of total void area to cross-sectional area for each polished sample. The composite panel thickness was measured along the laminate length using a micrometer. Fiber volume fraction (V_f) was calculated as $V_f = \frac{f_A n}{\rho_f t}$, where f_A and ρ_f are CF fabric properties (areal weight and fiber density, respectively), n is the number of plies, and t is the panel thickness. The fiber volume fractions reported in Table 1 were averaged over the center 5 cm of composite panels to correspond to the region measured by Instron video extensometer during tensile testing.

Glass transition temperature (T_g) was determined by dynamic mechanical analysis (DMA, TA Instruments RSA G2). Specimens 44 mm × 5 mm were cut parallel to the direction of front propagation and from two panel locations: near the resin outlet and at the panel mid-length (i.e. merged interface for two-front tests). DMA samples were then loaded in a three-point bend fixture and oscillated at 0.01% maximum strain at 1 Hz from 0 °C to 250 °C at 2 °C min^{-1}. Degree-of-cure (α) was characterized by differential scanning calorimetry (DSC) by slicing 6 mg samples from DMA specimens (prior to testing) and sealing in aluminum pans with hermetic lids. Residual exotherm was measured by heating samples from −50 °C to 250 °C at 2 °C min^{-1} in a TA Instruments Q20 DSC with CFL-50 cooling system. The α was calculated as $\alpha = 1 - \frac{H}{H_R}$, where H is the residual exotherm (corrected for matrix mass) and H_R is the enthalpy of reaction of the liquid resin system.

2.7. Mechanical characterization

For all FROMP composites, tensile specimens were prepared and tested according to ASTM D3039 to evaluate the effect of multiple-front polymerization on the mechanical properties of produced laminates. Previously reported bulk-cured pDCPD and epoxy composite tensile properties were included for reference [21]. Rectangular samples 203 mm × 13 mm were cut from the center of composite panels such that the loading direction was parallel to the direction of front propagation. For two-front composites, the mid-length of the tensile specimen corresponded to the merged interface. Tensile samples were end tabbed with G10 FR4 glass–fiber/epoxy tabs that were 45 mm × 13 mm × 0.2 mm with a 15° taper. End tabs and composite surfaces were lightly roughened to improve grip, then adhered together with JB weld adhesive and cured overnight at room temperature. Tensile samples were tested on an Instron 5984 with a 2 mm min^{-1} crosshead speed.

Strain was measured with an Instron video extensometer over a 5 cm region at the center of the tensile specimen. Tensile strength was calculated based on the maximum load achieved during testing and average nominal cross-sectional area of the sample over the center 5 cm region. Digital image correlation (DIC) was also used during testing to measure strain fields at the sample mid-length (i.e. merged interface in the two-front tests). DIC measurements were conducted by applying a 25 mm × 13 mm speckle pattern on the surface of the tensile specimens prior to testing. Images of the patterned surface were captured using a 5 megapixel camera at 1 Hz, then analyzed in a commercial DIC software (Vic-2D) according to the process outlined in [26].

2.8. Computational modeling

To provide insight on the interaction between the merging polymerization fronts, we performed 1D and 2D simulations of FROMP in CF/DCPD composites based on the following reaction–diffusion model written in terms of the temperature, T (in K), and degree-of-cure, α (non-dimensional), solutions [22]:

$$\begin{cases} \overline{\kappa}\nabla^2 T + \overline{\rho}(1-V_f)H_m\frac{\partial\alpha}{\partial t} = \overline{\rho C_p}\frac{\partial T}{\partial t}, \\ \frac{\partial\alpha}{\partial t} = A\exp(-\frac{E}{RT})(1-\alpha)^n\alpha^m\frac{1}{1+\exp(c_d(\alpha-\alpha_d))}, \end{cases} \quad (1)$$

where the overbar refers to the homogenized value of the composite property, the subscript 'm' corresponds to the resin matrix, κ (in W m^{-1} K^{-1}), ρ (in kg m^{-3}), and C_p (in J kg^{-1} K^{-1}) respectively denote the thermal conductivity, density, and specific heat capacity, H_m (in J kg^{-1}) is the enthalpy of the reaction, and V_f is the fiber volume fraction. The second relation corresponds to the cure kinetics model for which we adopted a modified Prout–Tompkins autocatalytic model [27], where A (in s^{-1}) is the Arrhenius time constant, E (in J mol^{-1}) is the activation energy, R (= 8.314 J mol^{-1} K^{-1}) is the universal gas constant, and n, m, c_d, and α_d are non-dimensional constants. Finite element method simulations were performed using the Multiphysics Object-Oriented Simulation Environment (MOOSE) to take advantage of the framework's robust mesh adaptivity needed to capture the high temperature and degree-of-cure gradients present in the vicinity of the moving polymerization front [25].

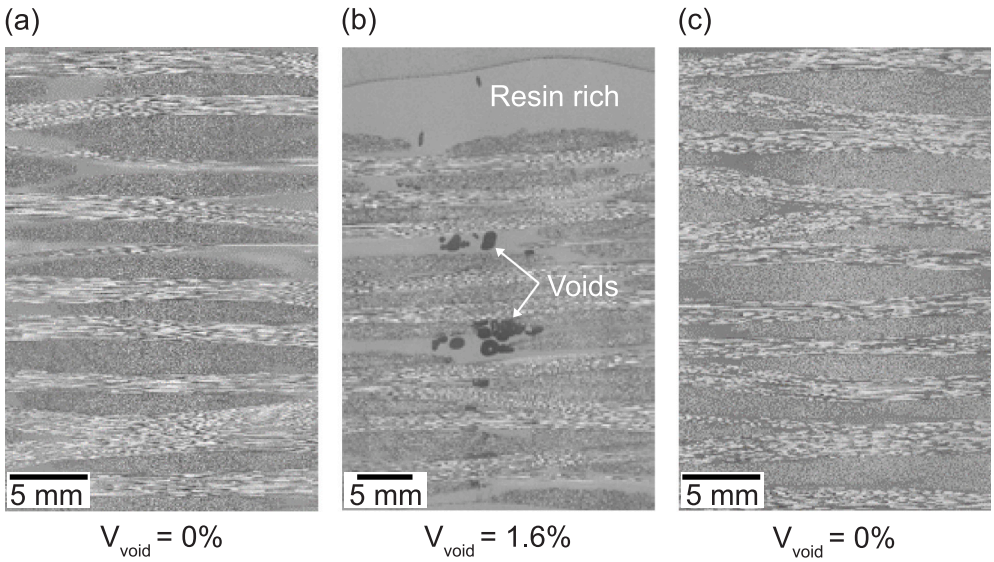

Fig. 5. Representative optical micrographs taken at the cross-section of panel mid-length for specimens fabricated using (a) one front with TIB, (b) two fronts with TIB, and (c) two fronts with TCB.

Table 2
Cure time, front speed, and energy input to manufacture FROMP composites compared to bulk-cured composites.[a,b]

Specimen	Cure time (min)	Front velocity (cm min^{-1})	Energy input (kJ)
One front TIB	5.4 ± 0.7	4.8 ± 0.7	4
Two fronts TIB	1.7 ± 0.2	6.0 ± 0.9[c]	8
Two fronts TCB	1.1 ± 0.1	10.4 ± 0.5	24
Bulk-cured pDCPD [21]	380	–	37,000
Bulk-cured epoxy [21]	480	–	45,000

[a]Error represents one standard deviation.
[b]Energy input for FROMP tests were calculated based on power ratings given by the heater supplier. Energy input for epoxy test was calculated based on measured energy consumption rates for a comparable thermal oven [8].
[c]Front velocity accelerated when two fronts were in proximity to each other, leading to shorter cure time than calculated with this value.

3. Results and discussion

Two-front composite panels were fabricated first using thermally insulated tool plates (TIB), similar to the method used for one-front panels [21]. Thermally conductive tool plates (TCB) were then adopted to mitigate processing issues associated with merging fronts. Properties of the two-front composites are compared to one-front composites and conventional hot press cured pDCPD and epoxy composites. The cure time, front velocity and required energy input for each of these composites are summarized in Table 2, and fiber volume fraction and tensile properties are summarized in Table 1.

3.1. Merged interface characterization

Cross-sections of one-front TIB composites revealed less than 0.5% void content throughout the entire panel volume (Fig. 5a). In contrast, two-front TIB composites had 2.0% (±1.8) void content at the merged interface in addition to a resin-rich layer on the top surface of the composite (Fig. 5b). The regions adjacent to the merged interface showed less than 0.5% void content. The localization of voids at the merged interface stemmed from the initiation of the second front that partially blocked the vacuum outlet. The partially closed outlet resulted in a greater volume of air, water, or other impurities to be entrapped within a two-front panel compared to a one-front panel where the vacuum outlet remained open for the duration of curing. We did not attribute the void formation in two-front TIB composites to the front temperature (maximum ca. 157 °C) because significantly hotter front temperatures (ca. 215 °C) were measured for neat DCPD with minimal voids in the cured polymer [21].

Table 3
Thermal conductivity, density, and specific heat capacity of DCPD and CF used for the simulations.

	κ (W m^{-1} K^{-1})	ρ (kg m^{-3})	C_p (J kg^{-1} K^{-1})
DCPD	0.15	980	1600
CF	10.45	1790	795

Table 4
Cure kinetics parameters of the Prout–Tompkins autocatalytic model Eq. (1) for DCPD.

n	m	c_d	α_d	A (s^{-1})	E (kJ mol^{-1})	H_m (J g^{-1})
1.72	0.77	14.48	0.41	8.55 e15	110.75	350.0

We measured a steady increase in panel thickness and corresponding decrease in fiber volume fraction along the panel length of two-front TIB composites, whereas one-front TIB composites showed thickness uniformity throughout. The normalized thickness values plotted in Fig. 6a were obtained by dividing the raw value at each normalized panel location (x) by the average panel thickness near the vacuum outlet (x = 1). The two-front TIB composites experienced a maximum thickness increase of 30% at the merged interface (x = 0.5). The thickness variation resulted from a combination of partial vacuum loss and resin flow during frontal curing. The initiation of the second front formed a section of solid material that partially blocked the vacuum outlet. Some amount of excess resin was entrapped within the layup and pushed ahead of the two fronts, accumulating at the panel mid-length. A literature review on neat FP systems [28] attributes this flow phenomenon to tension-driven convection at the interface between the resin and a free surface. Another possible contributor to the flow is

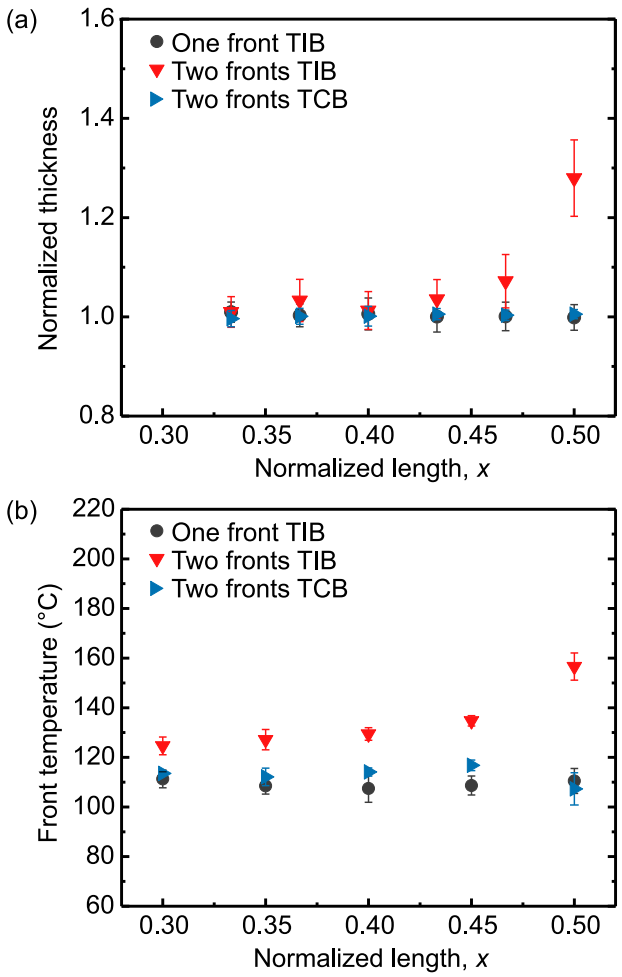

Fig. 6. (a) Normalized panel thickness and (b) *in-situ* front temperature measured at the laminate surface as a function of normalized panel length (x). For both plots, $x = 0$ and $x = 0.5$ correspond to the resin inlet and panel mid-length, respectively. The two-front TIB case showed an increase both in panel thickness and front temperature with the greatest values occurring at the merged interface ($x = 0.5$). Error bars represent one standard deviation from the mean ($n = 3$).

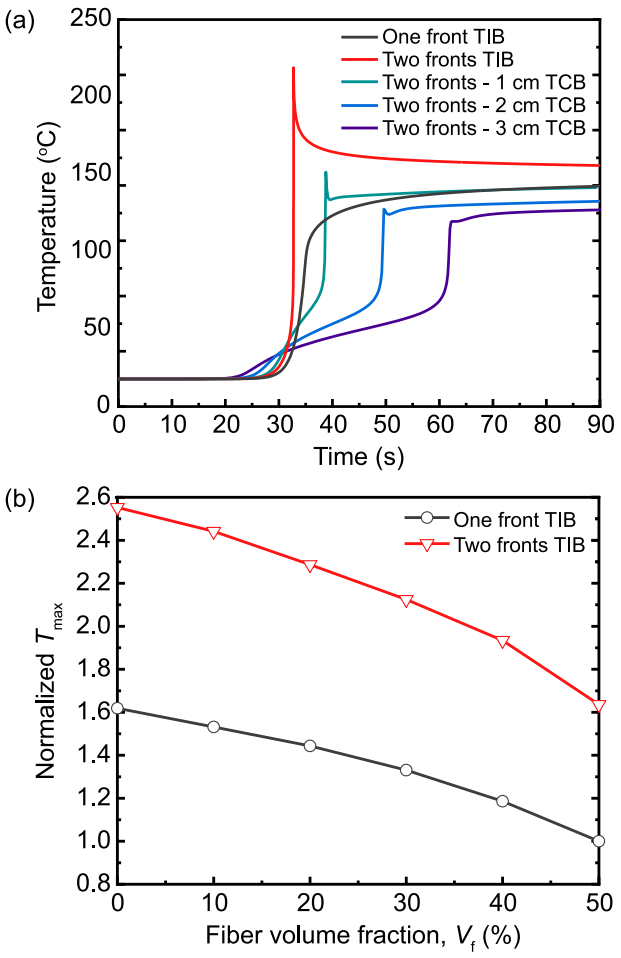

Fig. 7. (a) Computational predictions of temperature evolution associated with a single front (black curve) and two merging fronts (red curve) at the location of the front merger for CF/DCPD composites with $V_f = 0.5$. The separation between the two curves prior to the onset of the thermal spike (starting at time $t \approx 30$ s) illustrates the accelerated temperature rise due to the interaction between the two fronts. The green, blue, and purple curves show the effect of the length of the TCB on the thermal spike. (b) Computational predictions of maximum front temperature (normalized by the front temperature of a single front obtained for $V_f = 0.5$) as a function of the fiber volume fraction for the single front (black curve) and two-front (red curve) cases.

thermal expansion of the resin due to large thermal gradients during curing.

We also observed an increase in front temperature for two-front TIB panels similar to the thickness variation along the panel length. A thermal spike of 157 °C (±5.5) occurred at the merged interface ($x = 0.5$) (Fig. 6b). In contrast, the front temperature in one-front TIB composites was nearly constant at 110 °C (±2.9). One contributor to the formation of the thermal spike was the accumulation of excess heat between two merging fronts that was no longer being dissipated into uncured monomer. A second contributor to the higher temperature was the increased panel thickness, i.e. the increased monomer volume, along the panel length.

To understand the front temperature increase in the two-front TIB panels, we performed 1D (adiabatic) simulations for one-front and two-front cases. For the single-front case, these simulations were carried out with a domain length of 10 cm and a thermal trigger of 210 °C applied for 1 s at the left end of the domain. For the two-front case, symmetry conditions were adopted to capture the interaction of the two fronts in the middle of the domain. To explore the effects of the fiber volume fraction (V_f) on the temperature rise at the merged interface, we performed a set of 1D simulations based on a simple rule of mixtures used to homogenize material properties in Eq. (1) [22,29]. These simulations were carried out over the range $0.0 \leq V_f \leq 0.5$ using the aforementioned 1D domain and trigger. The material properties for the CF and DCPD resin used in these simulations are listed in Table 3, while the cure kinetics parameters of the resin are provided in Table 4.

Fig. 7a presents the evolution of temperature for one-front (black curve) and two-front (red curve) simulations when $V_f = 0.5$. In addition to the very rapid increase in temperature experienced at the exact front merging location, the results show an earlier rise in temperature for two fronts as they start interacting with each other. This acceleration of the fronts near the merger location was also observed in experiments.

As illustrated in Fig. 7b, and in agreement with results presented in [22], the maximum temperature (T_{max}) achieved in one-front and two-front simulations decreased with V_f. The normalized T_{max} values in Fig. 7b were obtained by dividing the front temperature recorded at the center of the domain (location of the thermal spike for two-front simulations) by the front temperature recorded for a one-front simulation with $V_f = 0.5$ (ca. 150 °C). Due to the adiabatic nature of the 1D simulations, the ratio of T_{max} for two-front to one-front simulations was ca. 1.6, which overestimated the experimentally observed value of 1.3. This T_{max} ratio remains nearly constant for all simulated values ($0.0 \leq V_f \leq 0.5$) despite the effect of increasing fiber content on the homogenized properties of the composite.

3.2. Front acceleration near the merged interface

Front velocities and cure times for one-front and two-front TIB composites are compared in Table 2. The one-front cases exhibited constant front velocities of ca. 5 cm min^{-1} over the entire laminate length of 30 cm. In contrast, the two-front cases exhibited higher front velocities of ca. 6 cm min^{-1} near the heat triggers (owing to lower V_f/higher monomer volume compared to the one-front panels) followed by an increase in velocity when the two fronts came in proximity to each other, i.e. nearing the merged interface (Fig. 4). Cure times were less than 2 min for 30 × 30 cm^2 two-front TIB composites compared to 5.4 min for one-front TIB panels of identical dimensions — a nearly 3-fold reduction in cure time for minimal additional energy input (Table 2). Numerical studies of similar FP systems have shown that the front velocity is a function of the initial temperature of the resin, front temperature, and monomer volume [22,25,30]. We hypothesized that the buildup of a resin rich region was the primary driver for the increase in front velocity in two-front TIB composites.

3.3. Effect of the merged interface on composite performance

One-front TIB composites exhibited a uniform glass transition temperature (T_g = 134 ± 0.6 °C) throughout the panel volume corresponding to a uniform degree-of-cure (α = 88 ± 2.6%). For two-front TIB composites, regions tested near the merged interface had a small, but statistically significant increase in T_g (138 ± 0.5 °C) compared to regions near the outlet (T_g = 136 ± 0.2 °C), with p = 0.03 (calculated by one-way analysis of variance (ANOVA)). The higher T_g at the merged interface was attributed to further crosslinking due to the thermal spike achieved during frontal curing, further supported by the small increase in α (92 ± 1.0%) compared to the one-front TIB tests.

Optical images of representative fractured specimens and tensile strengths for one-front and two-front TIB composites are shown in Fig. 8 and Table 1, respectively. Two-front TIB specimens had a 10% lower average tensile strength compared to one-front TIB samples, which may be attributed to the lower V_f as well as the concentration of voids at the mid-length of tensile specimens (corresponding to the merged interface). One-front TIB samples developed a fairly uniform strain field under tensile loading and failed at random locations along the specimen length (Fig. 8a). In contrast, DIC analysis of two-front TIB specimens showed consistent strain localization in the vicinity of the merged interface followed by failure at this location (Fig. 8b). The localized strain regions developed symmetrically about the merged interface during loading and likely originated from the combined effects of aforementioned merging fronts phenomena. The consistent failure behavior suggested that phenomena measured at the merged interface contributed to the reduction in tensile strength in two-front TIB specimens.

3.4. Two-front composites fabricated using thermally conductive boundaries (TCB)

We improved the tensile properties in two-front composites by mitigating the merged interface through modification of the layup boundary conditions. Although several different configurations were tested, here we discuss the most successful case for eliminating merged interface phenomena: a two-front layup with thermally conductive boundaries (TCB).

A simplified geometry of the modified two-front layup was simulated to probe the impact of TCB on the predicted thermal spike in the composite. As shown in Fig. 9a, the simulated problem consists of the top half of a symmetric, 10 cm long, 1.5 mm thick CF/DCPD composite panel (initially at 20 °C) with a 0.55 mm thick aluminum plate (initially at 20 °C) of length L_{metal}, which was varied hereafter in a parametric study. Fig. 9b presents three snapshots of the simulated temperature field as the two fronts merge below the metal plate with

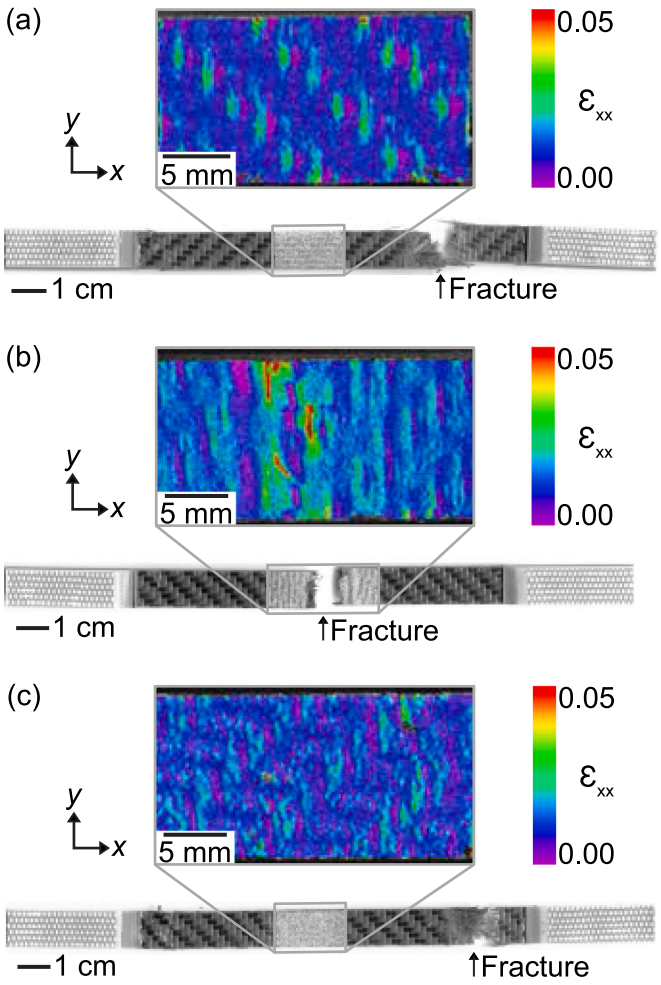

Fig. 8. Strain field of specimens under tensile loading just before fracture (top row) and optical image of specimens after fracture (bottom row) for (a) one-front TIB, (b) two-front TIB, and (c) two-front TCB tests. Two-front TIB specimens consistently failed at the merged interface.

L_{metal} = 1 cm. As expected, the hottest temperature values are obtained at the bottom of the composite domain (z = 0) at the merging location (x = 0). The evolution of the temperature in the middle of the domain ($x = z$ = 0) is compared for four values of L_{metal}. As apparent in Fig. 7a, the metal plate has two effects on the predicted thermal spike. Firstly, the maximum temperature decreases as L_{metal} increases. Secondly, the presence of the heat absorbing metallic layer also sharply reduces the duration of the spike, leading to the rapid cooling of the composite layer. Although simplified in the adopted geometry and boundary conditions, these simulations confirm the ability of the metallic strip to alleviate the thermal spike experienced by the composite material during two-front polymerization.

Two-front composite panels were manufactured using modified thermally conductive boundaries (TCB) as shown in Fig. 3. Constraining the VARTM layup with rigid aluminum plates enforced thickness uniformity throughout the panel volume (Fig. 6a). The combination of rigid and thermally conductive boundaries also eliminated the thermal spike, resulting in a uniform front temperature of 115 °C (±5.4) which closely matched front temperatures achieved in one-front TIB composites (Fig. 6b). We also achieved less than 0.5% void content throughout the modified two-front panel volume, which we attributed to the pressure applied on the layup surfaces that prevented expansion of any entrapped impurities (Fig. 5c). Finally, a slight increase in T_g (137 ± 0.2 °C) was measured in fully cured two-front TCB panels

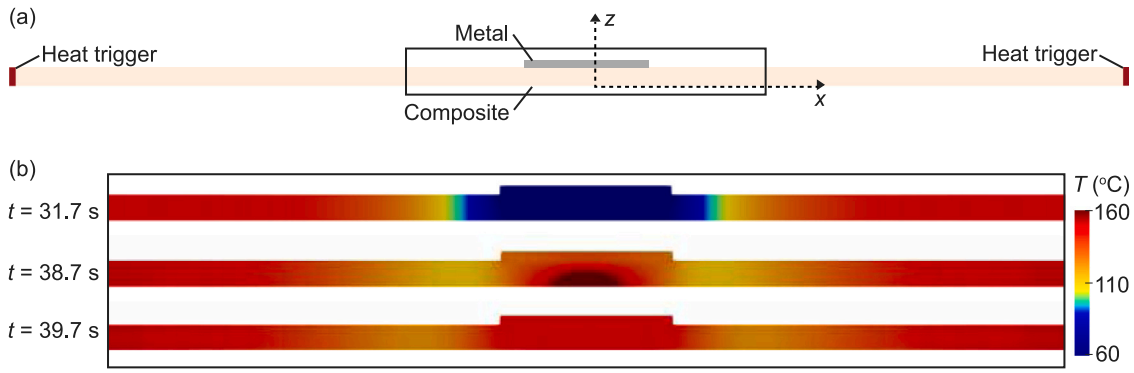

Fig. 9. (a) Schematic of the simulated composite (V_f = 0.5) used to capture the effect of the metallic boundary (initially at 20 °C) on the thermal spike created by merging fronts. Except for the duration of the thermal triggers applied on the left and right edges of the composite panel, all boundaries are assumed to be adiabatic. In all simulations, the thickness of the metallic strip is kept constant, while the length of the strip (L_{metal}) is varied. The coordinate system is indicated by the dotted arrows. (b) Temperature (T) contours obtained for L_{metal} = 1 cm. At t = 31.7 s, the fronts are steadily propagating towards each other. At t = 38.7 s, the fronts merge leading to a thermal peak of ca. 180 °C. A second later, at t = 39.7 s, the temperature at the location of the front merger has been substantially reduced due to the heat absorbed by the metallic strip.

compared to one-front TIB panels (T_g = 134 ± 0.6 °C). Interestingly, the elimination of the merged interface and slight increase in matrix crosslinking in two-front TCB specimens resulted in ca. 6% increase in tensile strength (656 ± 12 MPa) compared to one-front TIB specimens (618 ± 12 MPa) (Table 1). As shown in Fig. 8c, two-front TCB tensile samples also failed at random locations along the specimen length similar to one-front TIB samples.

The mitigation of the merged interface eliminated the front acceleration observed in two-front TIB composites. Even without the front acceleration, two-front TCB composites exhibited fast front velocities of ca. 10 cm min^{-1} (Fig. 4), thus achieving rapid cure times of ca. 1 min. The cure times for two-front TCB composites were 5× faster than one-front TIB composites and 1.5× faster than two-front TIB composites for an additional order of magnitude in energy input. Compared to bulk cured tests, two-front TCB tests achieved two and three orders of magnitude cure time and energy savings, respectively (Table 2). We hypothesized that the TCB tests achieved faster front velocities than TIB tests due to the preheating of the resin (relationship previously reported in a neat FP numerical study [30]) and/or the thermal properties of the tool plate. The higher thermal diffusivity of the metal boundaries (85 mm^2 s^{-1}) compared to insulator boundaries (0.2 mm^2 s^{-1}) may have accelerated the front at the laminate-boundary interfaces. In addition to producing composites with improved mechanical performance and faster cure times, the TCB layup is compatible with existing tooling in industry [31,32] and more complex trigger/front configurations.

4. Conclusions

We manufactured 30 × 30 cm^2 CF/pDCPD composite panels using one front and two fronts to investigate the effect of multiple-front polymerization on composite quality and tensile strength. Two-front panels manufactured using thermally insulated boundaries (TIB) achieved faster cure times for minimal additional energy input compared to one-front TIB panels. However, two-front TIB composites showed a knockdown in tensile strength due to a localization of voids, thickness increase, and thermal spike measured at the location of merging fronts (i.e. merged interface). Computational modeling of the thermal interaction between two fronts guided modification of the experimental layup to mitigate merged interface phenomena. Manufacturing two-front panels with thermally conductive boundaries (TCB) instead of insulated boundaries effectively eliminated the merged interface and improved the tensile strength compared to one-front TIB samples. Furthermore, two-front TCB panels measured the fastest cure times of all FP tests of ca. 1 min. Compared to conventional bulk-cured composites, two-front TCB panels achieved two and three orders of magnitude cure time and energy savings, respectively, for comparable tensile strengths.

CRediT authorship contribution statement

P.J. Centellas: Conceptualization, Methodology, Formal analysis, Investigation, Writing – original draft, Visualization. **M. Yourdkhani:** Conceptualization, Methodology, Writing – review & editing, Supervision. **S. Vyas:** Methodology, Software, Formal analysis, Writing – review & editing. **B. Koohbor:** Methodology, Formal analysis, Investigation, Writing – review & editing. **P.H. Geubelle:** Resources, Writing – review & editing, Supervision. **N.R. Sottos:** Resources, Writing – review & editing, Supervision, Funding acquisition.

Declaration of competing interest

The authors declare that they have no known competing financial interests or personal relationships that could have appeared to influence the work reported in this paper.

Acknowledgments

We gratefully acknowledge the support of the NSF LEAP HI, United States, grant #1933932 as well as partial support from the AFOSR Center for Excellence, United States: Self-Healing to Morphogenic Manufacturing award FA9550-20-1-0194. We thank Greg Milner and Lee Booher of the UIUC Talbot Lab machine shop for assistance with tensile samples preparation and Jenny Chu and Aditya Gupta for assistance with layup materials preparation. The authors extend gratitude to Prof. Scott White for helping to conceive this work, his guidance, and helpful discussions.

References

[1] Daniel IM, Ishai O. Engineering mechanics of composite materials. 2nd ed. Oxford University Press; 2006.
[2] Brøndsted P, Lilholt H, Lystrup A. Composite materials for wind power turbine blades. Annu Rev Mater Res 2005;35:505–38. http://dx.doi.org/10.1146/annurev.matsci.35.100303.110641.
[3] Friedrich K, Almajid AA. Manufacturing aspects of advanced polymer composites for automotive applications. Appl Compos Mater 2013;20:107–28. http://dx.doi.org/10.1007/s10443-012-9258-7.
[4] Karbhari VM, Seible F. Fiber reinforced composites – Advanced materials for the renewal of civil infrastructure. Appl Compos Mater 2000;7:95–124. http://dx.doi.org/10.1023/A:1008915706226.
[5] Kluge JNE, Lundström TS, Ljung A-L, Westerberg LG, Nyman T. An experimental study of temperature distribution in an autoclave. J Reinf Plast Compos 2016;35:566–78. http://dx.doi.org/10.1177/0731684415624768.
[6] Abliz D, Duan Y, Steuernagel L, L. Xie DL, Ziegmann G. Curing methods for advanced polymer composites - A review. Polym Polym Compos 2013;21:341–8. http://dx.doi.org/10.1177/096739111302100602.

[7] Hubert P, Fernlund G, Poursartip A. Autoclave processing for composites. In: Advani SG, Hsiao K-T, editors. Manufacturing techniques for polymer matrix composites (PMCs). Woodhead publishing series in composites science and engineering, Woodhead Publishing; 2012, p. 414–34. http://dx.doi.org/10.1533/9780857096258.3.414, [chapter 13].
[8] Witik RA, Gaille F, Teuscher R, Ringwald H, Michaud V, Månson J-AE. Economic and environmental assessment of alternative production methods for composite aircraft components. J Clean Prod 2012;29–30:91–102. http://dx.doi.org/10.1016/j.jclepro.2012.02.028.
[9] Bader MG. Selection of composite materials and manufacturing routes for cost-effective performance. Compos Part A 2002;33:913–34. http://dx.doi.org/10.1016/S1359-835X(02)00044-1.
[10] Innovating Clean Energy Technologies in Advanced Manufacturing, Tech. Rep. Department of Energy United States of America; 2015. [chapter 6].
[11] Malnati P, Sloan J. Fast and faster: Rapid-cure resins drive down cycle times. 2018, URL: https://www.compositesworld.com/articles/fast-and-faster-rapid-cure-epoxies-drive-down-cycle-times. [Online; posted 22 March 2018],
[12] Hexion, editor. Epoxy systems for structural components. 2021, Online; URL: https://www.hexion.com/en-us/applications/composites/automotive/structural.
[13] Huntsman, editor. Dynamic fluid compression molding. 2021, Online; URL: https://www.compositesone.com/wp-content/uploads/DFCM-White-Paper.pdf.
[14] Solvay, editor. Solvalite 750. 2021, Online; URL: https://www.solvay.com/en/product/solvalite-750.
[15] Silcock MD, Garschke C, Hall W, Fox BL. Rapid composite tube manufacture utilizing the QuickstepTM process. J Compos Mater 2007;41:965–78. http://dx.doi.org/10.1177/0021998306067261.
[16] Agius SL, Magniez KJC, Fox BL. Cure behaviour and void development within rapidly cured out-of-autoclave composites. Composites B 2013;47:230–7. http://dx.doi.org/10.1016/j.compositesb.2012.11.020.
[17] Davies LW, Day RJ, Bond D, Nesbitt A, Ellis J, Gardon E. Effect of cure cycle heat transfer rates on the physical and mechanical properties of an epoxy matrix composite. Compos Sci Technol 2007;67:1892–9. http://dx.doi.org/10.1016/j.compscitech.2006.10.014.
[18] Sangermano M, D'Anna A, Marro C, Klikovits N, Liska R. UV-activated frontal polymerization of glass fibre reinforced epoxy composites. Composites B 2018;143:168–71. http://dx.doi.org/10.1016/j.compositesb.2018.02.014.
[19] Sangermano M, Antonazzo I, Sisca L, Carello M. Photoinduced cationic frontal polymerization of epoxy–carbon fibre composites. Polym Int 2019;68:1662–5. http://dx.doi.org/10.1002/pi.5875.
[20] Tran AD, Koch T, Knaack P, Liska R. Radical induced cationic frontal polymerization for preparation of epoxy composites. Compos Part A 2020;132:1–8. http://dx.doi.org/10.1016/j.compositesa.2020.105855.
[21] Robertson ID, Yourdkhani M, Centellas PJ, Aw JE, Ivanoff DG, Goli E, et al. Rapid energy-efficient manufacturing of polymers and composites via frontal polymerization. Nature 2018;557:223–7. http://dx.doi.org/10.1038/s41586-018-0054-x.
[22] Goli E, Parikh NA, Yourdkhani M, Hibbard NG, Moore JS, Sottos NR, et al. Frontal polymerization of unidirectional carbon-fiber-reinforced composites. Compos Part A 2020;130:1–7. http://dx.doi.org/10.1016/j.compositesa.2019.105689.
[23] Kim C, Teng H, Tucker CL, White SR. The continuous curing process for thermoset polymer composites. Part 1: Modeling and demonstration. J Compos Mater 1995;29:1222–53. http://dx.doi.org/10.1177/002199839502900905.
[24] Kim C, White SR. The continuous curing process for thermoset polymer composites. Part 2: Experimental results for a graphite/epoxy laminate. J Compos Mater 1996;30:627–47. http://dx.doi.org/10.1177/002199839603000505.
[25] Goli E, Robertson ID, Geubelle PH, Moore JS. Frontal polymerization of dicyclopentadiene: A numerical study. J Phys Chem B 2018;122:4583–91. http://dx.doi.org/10.1021/acs.jpcb.7b12316.
[26] Koohbor B, Mallon S, Kidane A, Sutton MA. A DIC-based study of in-plane mechanical response and fracture of orthotropic carbon fiber reinforced composite. Composites B 2014;66:388–99. http://dx.doi.org/10.1016/j.compositesb.2014.05.022.
[27] Yang G, Lee JK. Curing kinetics and mechanical properties of endo-dicyclopentadiene synthesized using different Grubbs' catalysts. Ind Eng Chem Res 2014;53:3001–11. http://dx.doi.org/10.1021/ie403285q.
[28] Pojman JA. Frontal Polymerization, vol. 4. Amsterdam: Elsevier; 2012, p. 957–80. http://dx.doi.org/10.1016/B978-0-444-53349-4.00124-2, [chapter 4].
[29] Vyas S, Goli E, Zhang X, Geubelle PH. Manufacturing of unidirectional glass-fiber-reinforced composites via frontal polymerization: A numerical study. Compos Sci Technol 2019;184:1–6. http://dx.doi.org/10.1016/j.compscitech.2019.107832.
[30] Goldfeder PM, Volpert VA, Ilyashenko VM, Khan AM, Pojman JA, Solovyov SE. Mathematical modeling of free-radical polymerization fronts. J Phys Chem B 1997;101:3474–82. http://dx.doi.org/10.1021/jp962150v.
[31] Strong AB. Fundamentals of composites manufacturing: materials, methods, and applications. 2nd ed. Dearborn: Society of Manufacturing Engineers; 2008.
[32] Stewart R. New mould technologies and tooling materials promise advances for composites. Reinf Plast 2010;54:30–6. http://dx.doi.org/10.1016/S0034-3617(10)70110-7.